Ligand-Dependent Dynamics of the Active-Site Lid in Bacterial Dimethylarginine Dimethylaminohydrolase

Masooma Rasheed,[†] Christine Richter,[†] Liisa T. Chisty,[‡] John Kirkpatrick,[§] Martin Blackledge,[#] Martin R. Webb,[‡] and Paul C. Driscoll*,[†]

[†]Division of Molecular Structure and [‡]Division of Physical Biochemistry, MRC National Institute for Medical Research, The Ridgeway, Mill Hill, London NW7 1AA, United Kingdom

[§]Institute of Structural and Molecular Biology, Division of Biosciences, University College London, Gower Street, London WC1E 6BT, United Kingdom

[#]Protein Dynamics and Flexibility, Institut de Biologie Structurale, CEA, CNRS, UJF-Grenoble 1, 41 Rue Jules Horowitz, F-38027 Grenoble, France

ⓢ Supporting Information

ABSTRACT: The dimethylarginine dimethylaminohydrolase (DDAH) enzyme family has been the subject of substantial investigation as a potential therapeutic target for the regulation of vascular tension. DDAH enzymes catalyze the conversion of asymmetric N^η,N^η-dimethylarginine (ADMA) to L-citrulline. Here the influence of substrate and product binding on the dynamic flexibility of DDAH from *Pseudomonas aeruginosa* (PaDDAH) has been assessed. A combination of heteronuclear NMR spectroscopy, static and time-resolved fluorescence measurements, and atomistic molecular dynamics

simulations was employed. A monodisperse monomeric variant of the wild-type enzyme binds the reaction product L-citrulline with a low millimolar dissociation constant. A second variant, engineered to be catalytically inactive by substitution of the nucleophilic Cys249 residue with serine, can still convert the substrate ADMA to products very slowly. This PaDDAH variant also binds L-citrulline, but with a low micromolar dissociation constant. NMR and molecular dynamics simulations indicate that the active site "lid", formed by residues Gly17-Asp27, exhibits a high degree of internal motion on the picosecond-to-nanosecond time scale. This suggests that the lid is open in the apo state and allows substrate access to the active site that is otherwise buried. L-Citrulline binding to both protein variants is accompanied by an ordering of the lid. Modification of PaDDAH with a coumarin fluorescence reporter allowed measurement of the kinetic mechanism of the PaDDAH reaction. A combination of NMR and kinetic data shows that the catalytic turnover of the enzyme is not limited by release of the L-citrulline product. The potential to develop the coumarin−PaDDAH adduct as an L-citrulline sensor is discussed.
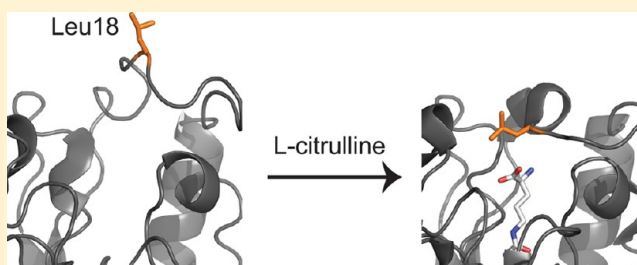
Vascular tension in mammals is maintained by arginine/nitric oxide signaling, regulated by isoforms of nitric oxide synthase (NOS) and their inhibitors.[1] NOS activity itself is regulated by the products of the catabolism of proteins containing methylated arginine that result from the action of protein-arginine methyl transferases. Specifically, the asymmetric N^η-methylated arginine amino acids L-N^η-monomethylarginine and asymmetric N^η,N^η-dimethylarginine (L-NMMA and ADMA, respectively) antagonize the action of NOS by competition with the substrate L-arginine and lead to an elevation in vascular tension. In healthy individuals, the levels of L-NMMA and ADMA are subject to the combined action of excretion via the kidneys and catabolism by isoforms of the enzyme dimethylarginine dimethylaminohydrolase (DDAH). DDAH converts L-NMMA or ADMA into the amino acid, L-citrulline, and methylamine or dimethylamine, respectively. Pharmacologic manipulation of DDAH activity affects vascular tension indirectly. As such, DDAH has been the subject of a substantial level of investigation as a potential therapeutic

target,[2−5] for example, to block synthesis of NO indirectly by the blockade of the degradation of naturally occurring NOS inhibitors in septic shock,[6] arthritis,[7] and some cancers.[8]

The therapeutic potential has led to the need to understand the structure and mechanism of DDAH enzymes in detail. Murray-Rust and co-workers solved the first three-dimensional X-ray crystal structure of a DDAH, from *Pseudomonas aeruginosa* (PaDDAH).[9] They reported details of wild-type PaDDAH in the apo state and of the active site Cys249Ser mutant in separate complexes with reaction substrate ADMA and product L-citrulline. The crystal structure of the Cys249Ser mutant revealed that the 254-residue protein chain is arranged like a propeller with five pseudosimilar modules as blades, each comprised of a three-stranded β-sheet packed against an α-helix

(Figure 1A). The overall pentein propeller is decorated with long variable loops occupying the top of the structure, as shown
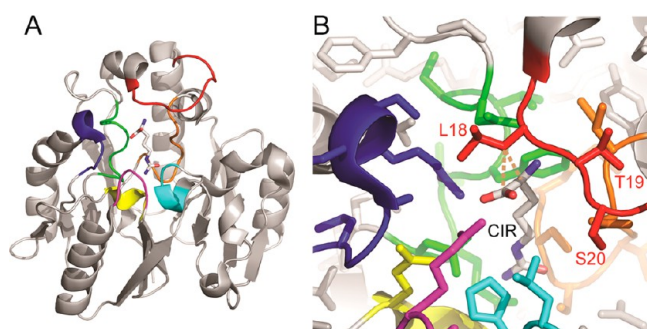

Figure 1. Three-dimensional structure of PaDDAH bound to L-citrulline showing the main features relevant to this work. (A) Ribbon representation of the crystal structure (PDB code 1H70) of the Cys249Ser mutant PaDDAH bound to L-citrulline. The ligand is shown in stick form with standard atom-type coloring. Loops that surround the active site chamber are depicted in color: red, loop 1 (L1); green, L2; blue, L3; yellow, L4; magenta, L5; cyan, L6; and orange, L7. (B) Close-up of the coordination of L-citrulline (CIR) by PaDDAH side chains. Protein side chain atoms (only) are displayed in stick representation and the color scheme is as in (A). The side chains of Leu18, Thr19, and Ser20 in L1 are labeled. Dashed lines (brown) indicate the van der Waals contact between the Cβ of Leu18 and the Cα and carboxylate carbon atoms of the ligand.

in Figure 1. The bound ligand resides in the center of the propeller, oriented along the propeller shaft axis with the distal end of the substrate side chain (the dimethyguanidinium group in the case of ADMA, the ureidyl group in the case of L-citrulline) sitting in a negatively charged pocket, made of Asp66, Glu65, and surrounded by a catalytic triad, comprising Glu114, His162, and Cys249 (Figure 1B). The ligand α-amino and carboxylate groups are braced on either side by H-bond interactions with the backbone carbonyl groups of Leu18 and Ile243 and salt bridge contacts with side chains of Arg85 and Arg132, respectively (Figure 1B). The ligand-binding site is covered by a loop (denoted L1, residues Gly17-Asp27) that lacks regular secondary structure (Figure 1A). The active site entrance is composed of an arrangement of loops between residues 54−67 (L2), 78−82 (L3), 107−113 (L4), 130−133 (L5), 157−161 (L6), and 243−251 (L7). The active site residues Glu114 and His162 lie in 3_{10}-helix segments, just adjacent to loops L4 and L6, and Cys249 lies in the L7 loop. Immediate egress of the ligand to solvent is apparently blocked by the position of the side chain of Leu18, the β-methylene group of which is in direct van der Waals contact with the α-CH moiety of the ligand (Figure 1B).

We previously demonstrated that PaDDAH forms a symmetric 58 kDa homodimer at concentrations required for biophysical and structural analysis.[10,11] Analytical size exclusion chromatography and sedimentation-equilibrium analytical ultracentrifugation (AUC) showed that self-association was sensitive to substitutions of surface amino acid residues without a significant impact on the observed level of catalytic activity. Locations for such substitutions were determined from the crystal structure, which displays contact between adjacent protein chains that conceals a total of 1720 Å² solvent accessible surface area. The equilibrium dissociation constant (K_{diss}) for the wild-type homodimer was determined by AUC to be 0.45 μM. The substitution, Asn36Trp, strengthened the

dimer slightly (K_{diss} = 0.26 μM), whereas mutations Arg40Glu or Arg98His significantly weakened the self-association: K_{diss} was 73 μM and 87 μM, respectively. The double mutant, Arg40Glu/Arg98His, displayed no detectable self-association and so provides a catalytically competent monomeric form of PaDDAH. This form of the protein shows excellent quality NMR spectra and so is a useful basis for detailed examination of the function and dynamics of the enzyme by heteronuclear NMR methods.[10]

Here we report the use of this double mutant PaDDAH (DM-PaDDAH) and its Cys249Ser variant triple mutant (TM-PaDDAH) that is almost completely inactive catalytically. These variants allow characterization of ligand binding and dynamic properties of the enzyme using NMR and fluorescence methods, supplemented with molecular dynamics (MD) simulations. A picture emerges of ligand-dependent ordering of the L1 loop. Incorporation of an environmentally sensitive fluorophore within this loop enabled the quantitative characterization of the enzyme mechanism. These data suggest that the rate-limiting step of the reaction, which is remarkably slow (k_{cat} ∼ 0.5 s⁻¹), is not release of the L-citrulline product but is attributable to an earlier step associated with the enzyme substrate interaction.

■ MATERIALS AND METHODS

Protein Expression and Purification. The preparation of wild-type PaDDAH and DM-PaDDAH has been described previously.[9,11] For this work, a pPROEX Hta plasmid encoding TM-PaDDAH was obtained by site-directed mutagenesis of the Cys249 codon using QuikChange site-directed mutagenesis (Agilent Technologies). Similarly, variants of both DM- and TM-PaDDAH were obtained, harboring additional Cys substitutions for coupling to a fluorophore label (see below).

PaDDAH proteins were expressed in *Escherichia coli* BL21 (DE3) cells at 37 °C, following induction with isopropyl-β-D-thiogalactopyranoside. Uniformly ^{15}N- and ^{15}N, ^{13}C-labeled proteins were prepared using an M9 culture medium containing ^{15}N$_2$-ammonium sulfate and ^{13}C$_6$-glucose as the sole nitrogen and carbon sources. Protein purification was performed using immobilized Ni-ion affinity chromatography (Ni Sepharose High Performance, GE Healthcare), polyhistidine affinity tag removal with TEV protease, removal of the affinity tag by a second Ni-affinity step, followed by semipreparative size-exclusion chromatography (Superdex 200, GE Healthcare) in 20 mM sodium phosphate buffer pH 7.0, 100 mM NaCl, 1 mM EDTA (buffer A).

NMR Spectroscopy. For NMR measurements, the protein samples were prepared at 0.8 mM concentration (for resonance assignments and relaxation measurements) or 0.3 mM (for ligand titrations) in buffer A, supplemented with 10% v/v D$_2$O. Saturating concentrations of L-citrulline were included in the bound state samples: 15 mM for DM-PaDDAH and 1.0 mM for TM-PaDDAH. A variety of NMR spectrometers were used during this work: resonance assignments were obtained from 3D triple resonance data sets (HNCA, HNCACB, CBCA-CONH, HNCO, HN(CA)CO)[12] obtained at either 600 or 700 MHz ^{1}H frequency. Two-dimensional ^{15}N, ^{1}H-HSQC experiments to monitor ligand binding were recorded using a 700 MHz instrument. ^{15}N relaxation measurements[13,14] were performed at both 600 and 800 MHz. The majority of the data sets were recorded using a cryogenically cooled triple resonance probe, with the sample temperature maintained at a calibrated 25 °C. The pulse sequences employed H$_2$O-selective

"flip-back" pulses and WATERGATE to minimize the effects of H^N-resonance cross-saturation.[15,16] Ligand-induced chemical shift perturbations differences for ligand titrations were computed using the formula $\Delta\delta = [(\Delta\delta^1H^N)^2 + (\Delta\delta^{15}N/5)^2]^{1/2}$.

^{15}N Longitudinal (R_1) and transverse (R_2) relaxation rate constants and $\{^1H\}^{15}N$ heteronuclear nuclear Overhauser enhancements (hNOEs) were recorded for apo and L-citrulline bound states of DM-PaDDAH and TM-PaDDAH at two field strengths, B_0 = 14.1 T (^1H frequency 600 MHz) and 18.8 T (^1H 800 MHz), using pulse sequences based upon those of Kay et al.[13] with embellishments described by Farrow et al.[14] Peak intensity errors were estimated from selected data sets with replicated relaxation delays. Spectra were acquired at 25 °C using 2000 × 240 and 2048 × 360 complex points in the $t_2 \times t_1$ dimensions at ^1H frequencies of 600 and 800 MHz respectively, with 16−48 scans per t_1 increment, a recycle delay of 1.4 s in R_1 and R_2 experiments, and a recycle delay of 1.2 s added prior to the 3.9 s ^1H saturation period in the hNOE experiments. The spectral widths in the direct and the indirect dimensions were 10000 × 2000 and 12000 × 3242 Hz at ^1H proton frequencies of 600 and 800 MHz, respectively.

NMR data were processed using NMRpipe package[17] and analyzed in CCPN analysis software.[18,19] The data were analyzed in terms of the model-free formalism[20,21] implemented in a version of TENSOR 2.0,[22] modified to perform simultaneous fitting of data obtained at multiple field strengths (Blackledge, M., unpublished data). Essentially identical results were obtained using MODELFREE.[23,24] Protons were built onto the crystallographic coordinates using MOLMOL.[25]

MD Simulations. Explicit solvent molecular dynamics simulations of apo and L-citrulline-bound DM-PaDDAH were performed in Particle-Mesh-Ewald periodic boundary mode using AMBER11,[26,27] broadly according to the protocols adopted by Palmer and co-workers.[28] Namely, the coordinates of the Cys249Ser PaDDAH/L-citrulline complex crystal structure (PDB code 1H70) were mutated in silico to include the substitutions Arg40Glu, Arg98His, and Cys249Ser. The structure was minimized and solvated in a truncated octahedral box of ~7000 TIP3P water molecules with a minimum distance of 11 Å from box boundary to any protein atom. Crystallographically observed water molecules were retained. Six sodium ions were strategically added to achieve charge neutrality. The total number of atoms was ~24 950. Following separate minimization of the solvent and intact system and regularization of the temperature (298 K) at constant volume and pressure, a 20 ns simulation at constant pressure and temperature (NPT) was used for equilibration. Multiple 20 ns NPT simulations were performed using the AMBER ff99SBILDN force field using a nonbonded cutoff of 10 Å, the SHAKE algorithm to constrain vibrations of bonds involving H-atoms, and an integration time step of 2 fs. Force field parameters for L-citrulline were generated using the R.E.D. Server[29,30] and the Antechamber tools in AMBER. For the apo-DM-PaDDAH simulation, the crystallographic coordinates of the L-citrulline ligand were removed prior to the solvation step. Visual inspection of the starting model validated the presence of several water molecules in the ligand binding cavity. Generalized order parameters for NH bonds (S^2) were calculated using a method that accounts for the effects of rare conformational transitions on the bond vector orientation autocorrelation functions, described by Palmer and co-workers,[31] from independent 4-ns trajectory slices.

Fluorophore Labeling. DM- or TM-PaDDAH constructs were mutated to contain an additional, solvent-exposed Cys residue at residue positions corresponding to Thr19, Ser 20, Ser84, and Asp244. Following expression, the purified proteins were each incubated in buffer A with 1 mM dithiothreitol (DTT) for 0.5 h. The sample was then passed through a desalting PD-10 column (GE Healthcare) in buffer A and concentrated to 100 μM. N-[2-(1-Maleimidyl)ethyl]-7-(diethylamino)coumarin-3-carboxamide (MDCC)[32] dissolved in DMF (20 mM) was added to a 2-fold excess, and the solution was incubated for 1 h. The reaction mixture was passed again through a fresh desalting column to remove unreacted label. The labeled protein concentration was measured by spectrophotometry (ε_{430} (MDCC) = 46 800 M^{-1} cm^{-1}, ε_{280}(MDCC) = 7470 M^{-1} cm^{-1}, ε_{280}(PaDDAH) = 18 910 M^{-1} cm^{-1}). Formation of the product was assessed by electrospray ionization mass spectrometry. Control experiments in which the coupling reaction was carried out with DM-PaDDAH (i.e., lacking an additional Cys residue) yielded no reaction with the MDCC coupling reagent, indicating that none of the other cysteines in the protein are sufficiently solvent accessible to react with the fluorophore. On the basis of this result and the spectrophotometric measurements, the level of labeling was in the 70−100% range.
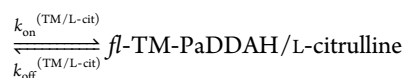
Fluorescence Measurements. PaDDAH fluorescence spectra were measured at 25 °C on an FP-6300 spectrofluorometer (Jasco Ltd.) in buffer A. MDCC fluorescence was excited at 430 nm and emission was recorded at 476 nm. The change in fluorescence emission intensity with ligand concentration was fit to a 1:1 binding isotherm using nonlinear least-squares Python code written in-house.

Stopped-flow experiments were carried out in buffer A at 25 °C using a HiTech SF61 DX2 stopped-flow instrument equipped with a Xe/Hg lamp (TgK Scientific, UK). MDCC fluorescence was excited at 436 nm, and emission was detected by a photomultiplier after a 455 nm cutoff filter (Schott glass). Protein (1 μM) was mixed with the ligand (ADMA or L-citrulline) at various concentrations up to 4 mM. In the mixing cell, concentrations were half these. Each fluorescence time course was fitted to a single exponential function

$$\Delta F(t) = \Delta F_{max}(1 - \exp(-k_{obs}t))$$

with the observed first-order rate constant, k_{obs}, and maximum fluorescence change, ΔF_{max}.

For mixing L-citrulline with MDCC-Ser20Cys TM-PaDDAH (fl-TM-PaDDAH), the dependence of k_{obs} on L-citrulline concentration ([L-cit]) was linearly fitted for the association reaction:

$$fl\text{-TM-PaDDAH} + \text{L-citrulline}$$

$$\underset{k_{off}^{(TM/L\text{-}cit)}}{\overset{k_{on}^{(TM/L\text{-}cit)}}{\rightleftharpoons}} fl\text{-TM-PaDDAH/L-citrulline}$$

$$k_{obs}^{(TM/L\text{-}cit)} = k_{on}^{(TM/L\text{-}cit)}[\text{L-cit}] + k_{off}^{(TM/L\text{-}cit)}$$

For the mixing of L-citrulline with MDCC-Ser20Cys DM-PaDDAH (fl-DM-PaDDAH) conversion of the substrate to products is included, using this reaction scheme:
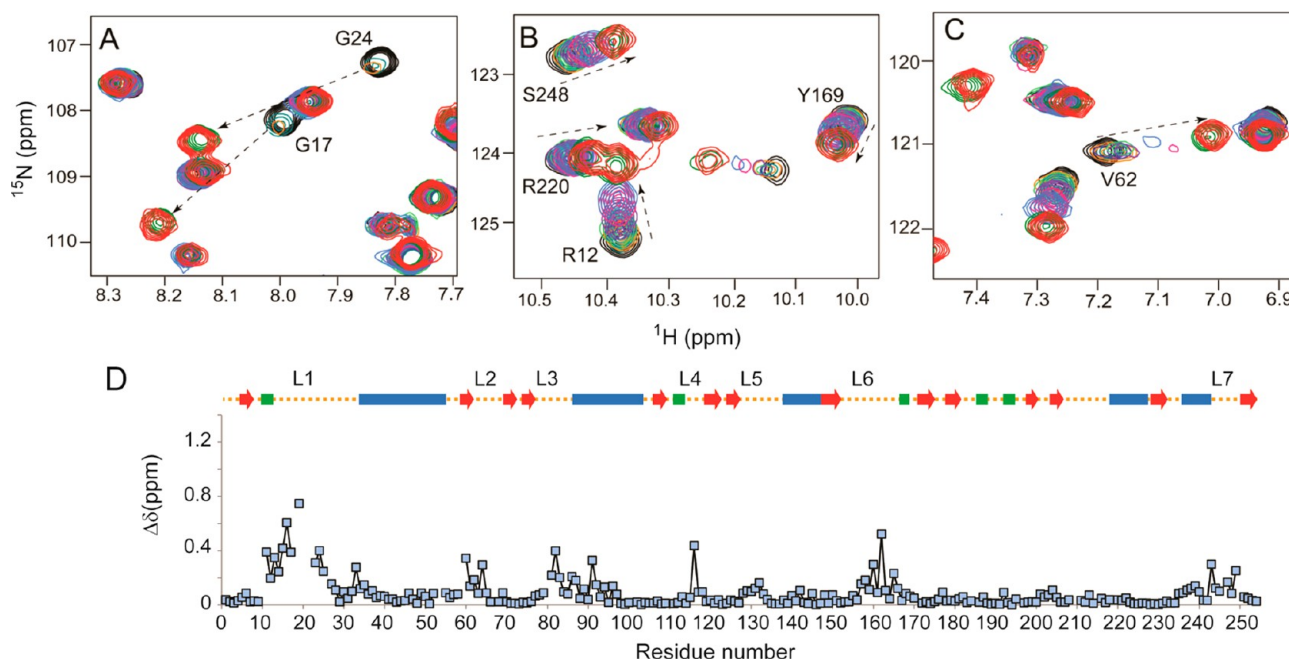
$$fl\text{-DM-PaDDAH} + \text{ADMA}$$

$$\underset{k_{off}^{(DM/ADMA)}}{\overset{k_{on}^{(DM/ADMA)}}{\rightleftharpoons}} fl\text{-DM-PaDDAH/ADMA}$$

Figure 2. NMR titration of DM-PaDDAH with L-citrulline. (A−C) Selected regions of the ^{15}N, ^{1}H-HSQC spectrum of 0.3 mM DM-PaDDAH recorded in the presence of different concentrations of L-citrulline. Dashed arrows indicate the chemical shift perturbation from the spectrum of the apo protein (black) to the effectively saturated complex (red). The concentration of L-citrulline in each spectrum was 0 mM (black), 0.6 mM (teal), 1.8 mM (orange), 3.0 mM (light green), 5.4 mM (purple), 8.7 mM (magenta), 13.8 mM (blue), 15.9 mM (dark green), and 20.7 mM (red), respectively. (D) Combined chemical shift ^{15}N, ^{1}H perturbation ($\Delta\delta$) plotted as a function of residue number. The secondary structure of PaDDAH is depicted at the top of the graph. The vertical scale is matched to that of Figure 3D. Values of $\Delta\delta$ for residues Leu18 and Ser20 were not measurable as the bound-state cross peaks are broadened beyond detection even at the highest loading of L-citrulline.

$$\xrightarrow{k_{cat}} fl\text{-DM-PaDDAH} + \text{L-citrulline} + \text{DMA}$$
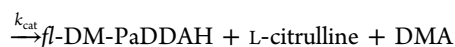
where k_{cat} is the rate constant for the conversion of the enzyme−substrate complex to dissociated products. Under the pseudo-first-order conditions of the experiment, where the change in fluorescence was attributed to the formation of the *fl*-DM-PaDDAH/ADMA complex, the dependence of k_{obs} on ADMA concentration was fitted to a straight-line graph:

$$k_{obs}^{(DM/ADMA)} = k_{on}^{(DM/ADMA)}[ADMA] + k_{off}^{(DM/ADMA)}$$
$$+ k_{cat}$$

■ RESULTS

Resonance Assignments. We have previously reported the backbone resonance assignments of the 254 residue DM-PaDDAH by triple resonance NMR using a uniformly ^{2}H, ^{13}C, ^{15}N-labeled sample.[10] The 2D ^{15}N, ^{1}H-HSQC spectrum of TM-PaDDAH that contains the additional substitution Cys249Ser is highly similar to that of DM-PaDDAH. Nevertheless, because of the relatively large number of cross peaks and the potential for misassignment by homology, we performed an independent, ab initio, triple-resonance-based, backbone resonance assignment for TM-PaDDAH. This could be achieved straightforwardly without recourse to the perdeuteration that we had employed previously. Comparison of the two sets of assignments resolved some minor ambiguities for both proteins with a small number of corrections to the deposited chemical shifts for DM-PaDDAH. Overall the assignment coverage (>97% of expected cross peaks) was excellent; none of the resolvable amide NH cross peaks was unattributed, and only a few residues had no detectable NH (Ser21, His22 in loop L1, and

Gly246 in loop L7), presumably due to exchange broadening. Three amide NH cross peaks appeared close to the solvent H$_2$O resonance: Glu171 (H^N; 4.30 ppm), Asn209 (H^N; 5.11 ppm), and Glu210 (H^N 5.03 ppm). The strong upfield shift was consistent with the close proximity of the amide H^N of Glu171 to the aromatic ring of Tyr169, and the amide H^N of Asn209 and Glu210 to the ring of Trp207. Chemical shift differences between DM- and TM-PaDDAH were localized to those residues lining the active site cavity. The invariance of the vast majority of chemical shifts indicated that the overall structure of the two proteins was very similar. Moreover, analysis of the ^{13}Cα/^{13}Cβ secondary chemical shifts in terms of predicted secondary structure showed that the patterns were entirely consistent with the protein architecture, observed for the single mutant, Cys249Ser PaDDAH protein in crystallo.

Ligand-Binding Titrations. Step-wise titration of DM-PaDDAH with substrates L-NMMA or ADMA yielded series of spectra that were essentially indistinguishable from those obtained by titration with the reaction product, L-citrulline. In these experiments, the chemical shifts of a subset of cross peaks displayed monotonic changes consistent with ligand binding with a dissociation rate on the fast-intermediate time scale (Figure 2A). This indicated that DM-PaDDAH was active and that the end-state of the measurements with substrates was the L-citrulline, product-bound state. Separate NMR titrations showed that the byproduct methylamine (from L-NMMA) or dimethylamine (from ADMA) did not detectably bind to the protein.

Most assignments of the L-citrulline-bound DM-PaDDAH could be obtained simply by monitoring the chemical shift trajectory during the titration (Figure 2A−C). However, for a subset of cross peaks (e.g., Gly17, Gly24, Figure 2A) the
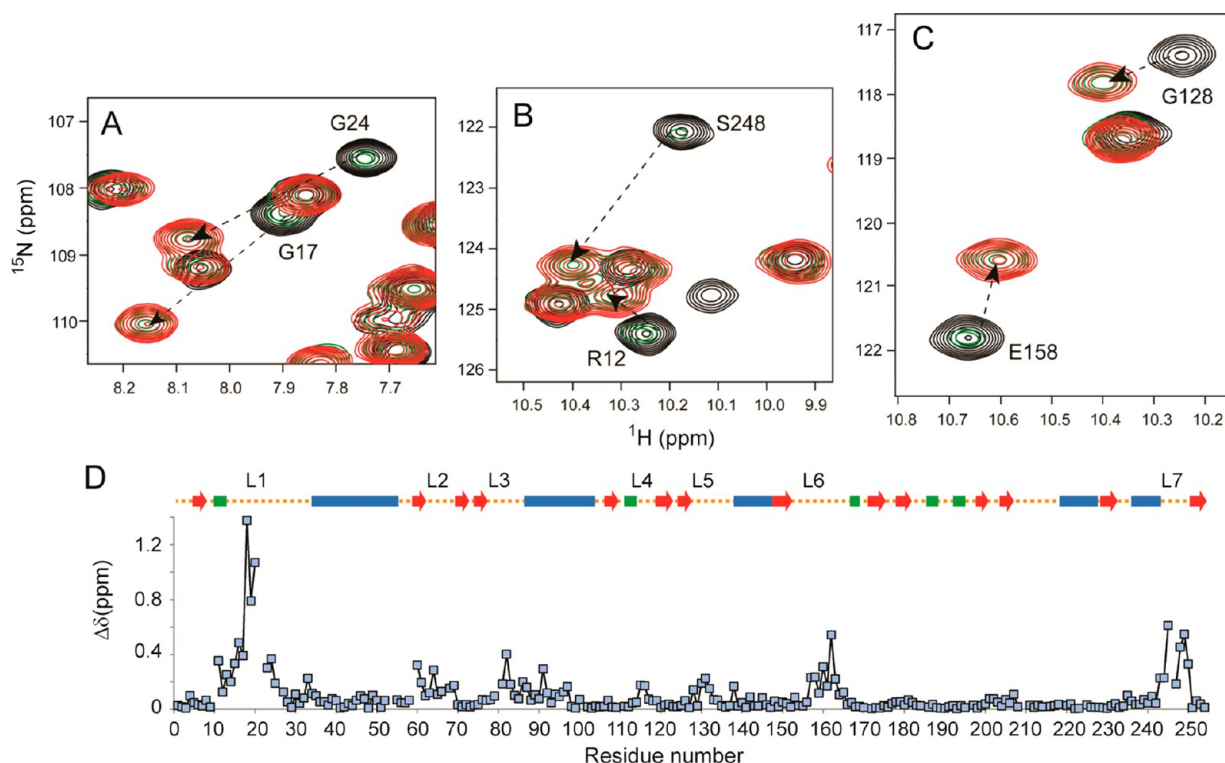
Figure 3. NMR titration of TM-PaDDAH with L-citrulline. (A−C) Selected regions of the ^{15}N, ^1H-HSQC spectrum of 0.3 mM TM-PaDDAH recorded in the presence of different concentrations of L-citrulline. Dashed arrows indicate the chemical shift perturbation from the spectrum of the apo protein (black) to the effectively saturated complex (red). The concentration of L-citrulline in each spectrum was 0 mM (black), 0.18 mM (dark green), and 0.46 mM (red), respectively. (D) Combined chemical shift ^{15}N, ^1H perturbation ($\Delta\delta$) plotted as a function of residue number. The secondary structure of PaDDAH is depicted at the top of the graph.
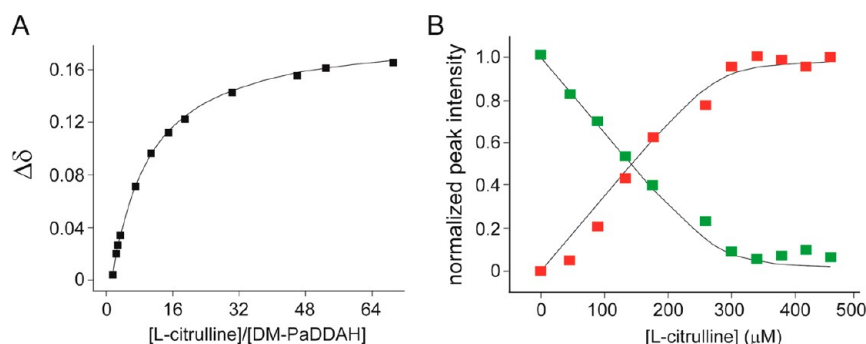

Figure 4. Ligand-dependent effects on the NMR spectrum of DM- and TM-PaDDAH proteins. Nonlinear best fits of the L-citrulline-dependent change in (A) combined ^{15}N, ^1H chemical shifts and (B) apo (green squares) and bound (red squares) cross peak intensities for 0.3 mM DM-PaDDAH and TM-PaDDAH, respectively. In each case, data points are aggregated over a small number of well-resolved cross peaks. The fitted values of the DM-PaDDAH/L-citrulline and TM-PaDDAH/L-citrulline dissociation constants are $K_D^{(DM/L\text{-cit})}$ = 3.6 ± 0.1 mM and $K_D^{(TM/L\text{-cit})}$ = 3.5 ± 1.5 μM, respectively.

titration was characterized by an almost immediate signal disappearance at low ligand concentration. The recovery of apparently new cross peaks at distinct positions in the spectrum occurred only at very high loading of the ligand, making transfer of assignment from free to bound state ambiguous. This ambiguity was resolved by a subset of triple-resonance NMR spectra for DM-PaDDAH saturated with L-citrulline that gave an almost complete assignment for the bound state. Notably, NH group assignments could not be obtained in the bound state for residues Leu18 and Ser20 in loop L1, and the NH cross peaks for residues in the C-terminal portion of loop L6 remain somewhat broader than the remainder.

For residues exhibiting fast-exchange behavior (e.g., Figure 2A−C), fits of the change in chemical shift to a model of 1:1 PaDDAH/L-citrulline complex formation yielded an estimate of the dissociation constant $\left(K_D^{(DM/L\text{-cit})}\right)$ of 3.6 ± 0.1 mM (Figure 4A). Interestingly, use of this value in simulations of titration spectra for amides exhibiting intermediate exchange, concomitant with the larger overall chemical shift perturbation, accurately reproduced the observed dependence of the cross-peak position and line shape profiles (Rasheed, M. et al., unpublished result). This indicated that the differing behaviors, observed for specific cross peaks, were attributable to a simple two-site exchange process without long-lived intermediates. Figure 2D shows the L-citrulline-dependent chemical shift
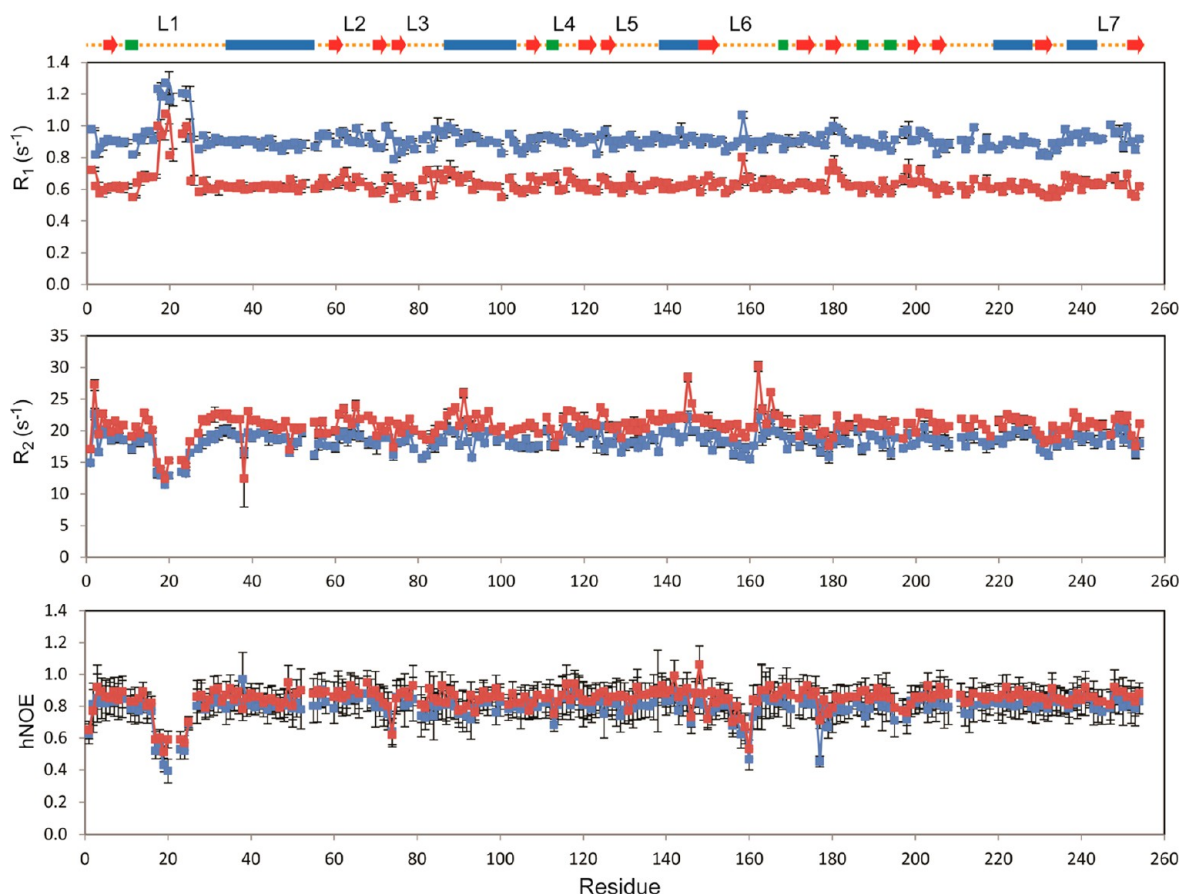
Figure 5. ^{15}N nuclear relaxation measurements for apo DM-PaDDAH. Per-residue ^{15}N R_1, ^{15}N R_2, and $\{^1H\}^{15}N$ heteronuclear NOE (hNOE) values obtained at ^1H 600 MHz (blue) and 800 MHz (red) and 25 °C. The secondary structure of PaDDAH is depicted at the top of the figure.

changes for DM-PaDDAH plotted per residue. These changes occurred in regions lining the active site pocket and particularly in loops L1–L7 that represent the ligand-binding site. The largest chemical shift changes occurred for residues in the N-terminal arm of loop L1, with the highest value displayed by Thr19.

Substrate and product titrations were also performed with TM-PaDDAH. With L-NMMA and ADMA there were slow ligand- and time-dependent changes in the spectrum of the protein−ligand mixtures that were consistent with turnover of the substrate. This interpretation was supported by observation of the TM-PaDDAH-dependent production of L-citrulline and methyl- or dimethylamine in the one-dimensional ^1H NMR spectrum. Thus, despite the removal of the catalytic thiol by Cys249Ser mutation, TM-PaDDAH retained weak catalytic activity, detectable at the high protein concentrations used for these NMR experiments. On the other hand, titration of TM-PaDDAH with L-citrulline gave rise to classic two-site, slow-exchange behavior (Figure 3A−C). Fitting the change in a subset (Gly24, Glu158, Lys159) of peak intensities as a function of ligand concentration yielded an estimate of the dissociation constant for the TM-PaDDAH/L-citrulline complex ($K_D^{(TM/L\text{-}cit)}$) of 3.5 ± 1.5 μM (Figure 4B).

The backbone chemical shifts of L-citrulline-saturated TM-PaDDAH were obtained by analysis of triple resonance NMR data sets recorded on a ^{13}C, ^{15}N-labeled protein sample. Figure 3D shows that the pattern of amide NH chemical shift changes upon binding L-citrulline is similar to that for DM-PaDDAH (Figure 2D), with the largest changes occurring for loops L1,

L6, and L7. As with DM-PaDDAH, the most highly perturbed cross peaks are those that derive from the N-terminal segment of loop L1. In this case, assignments of the NH groups of both Leu18 and Ser20 in the bound state could be unambiguously identified; these two residues displayed the highest values of L-citrulline-dependent chemical shift perturbation of the whole protein. This observation is relevant to the interpretation of the corresponding behavior for DM-PaDDAH: the intermediate exchange regime that pertains to those cross-peaks with the largest chemical shift differences could lead to a situation in which exchange broadening persists even in the presence of a very significant excess of L-citrulline. This broadening rationalizes the failure to detect NH cross peaks for Leu18 and Ser20 in the spectrum of L-citrulline-bound DM-PaDDAH.

Dynamics by NMR. Backbone dynamics of ligand-free (apo) and L-citrulline-saturated DM- and TM-PaDDAH proteins were measured using nuclear relaxation measurements recorded at two field strengths. The R_1, R_2, and hNOE values were plotted per residue for apo and L-citrulline saturated DM-PaDDAH in Figures 5 and 6, respectively. The corresponding data for apo and L-citrulline-bound TM-PaDDAH were highly similar (Figures 1 and 2 of the Supporting Information). The data were analyzed in terms of the model-free formalism[20,21] using essentially standard procedures.[13,23] The effective overall rotational correlation time (τ_c) for the protein was estimated from the set of ^{15}N R_2/R_1 ratios, trimmed for outliers. The data for the four samples yielded τ_c in the range 13.7−14.4 ns in line with expectations for a 28 kDa protein at 25 °C. Using the crystallographic coordinates of Cys249Ser PaDDAH (PDB
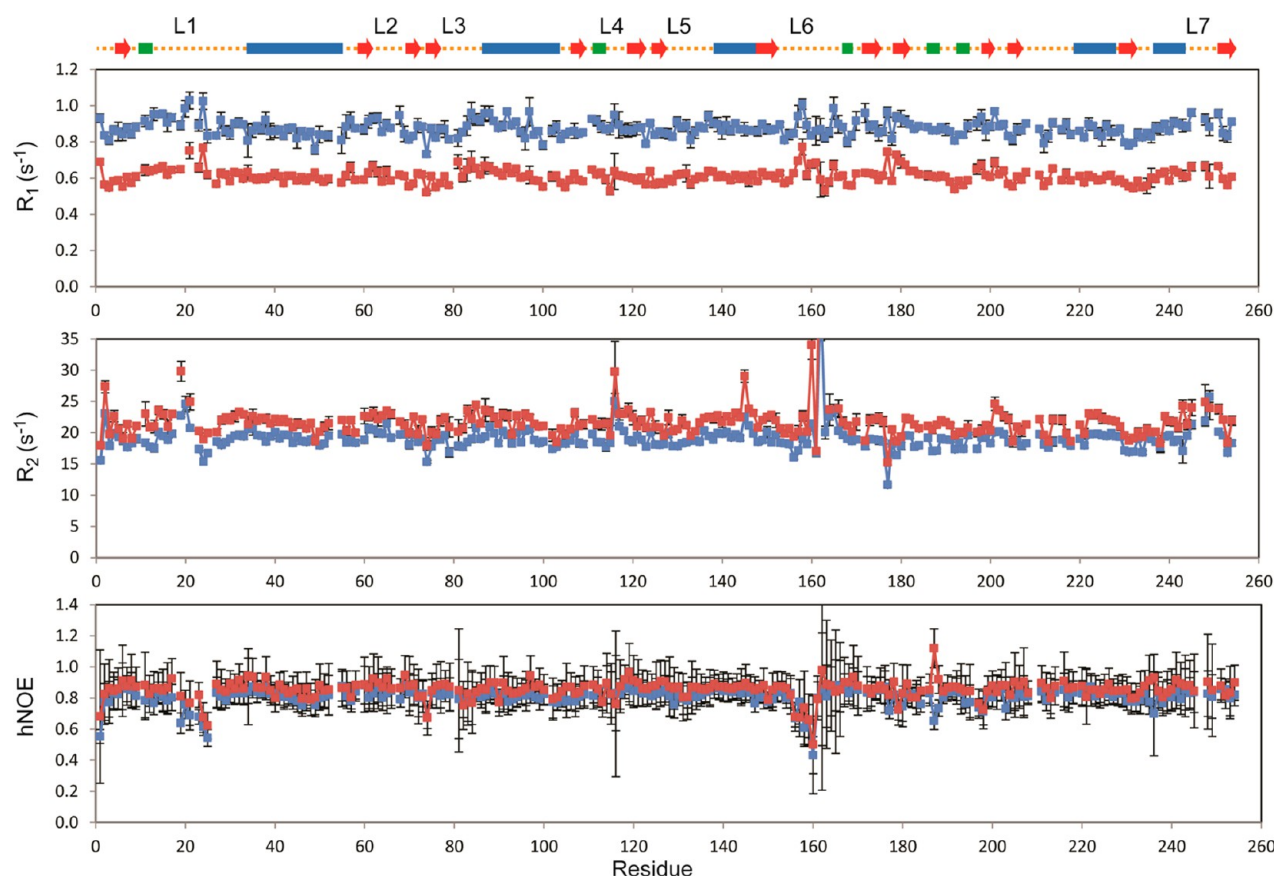
Figure 6. ^{15}N nuclear relaxation measurements for L-citrulline-saturated DM-PaDDAH. Per-residue ^{15}N R_1, ^{15}N R_2, and {^{1}H}^{15}N heteronuclear NOE (hNOE) values obtained at ^{1}H 600 MHz (blue) and 800 MHz (red) and 25 °C. The secondary structure of PaDDAH is depicted at the top of the figure.
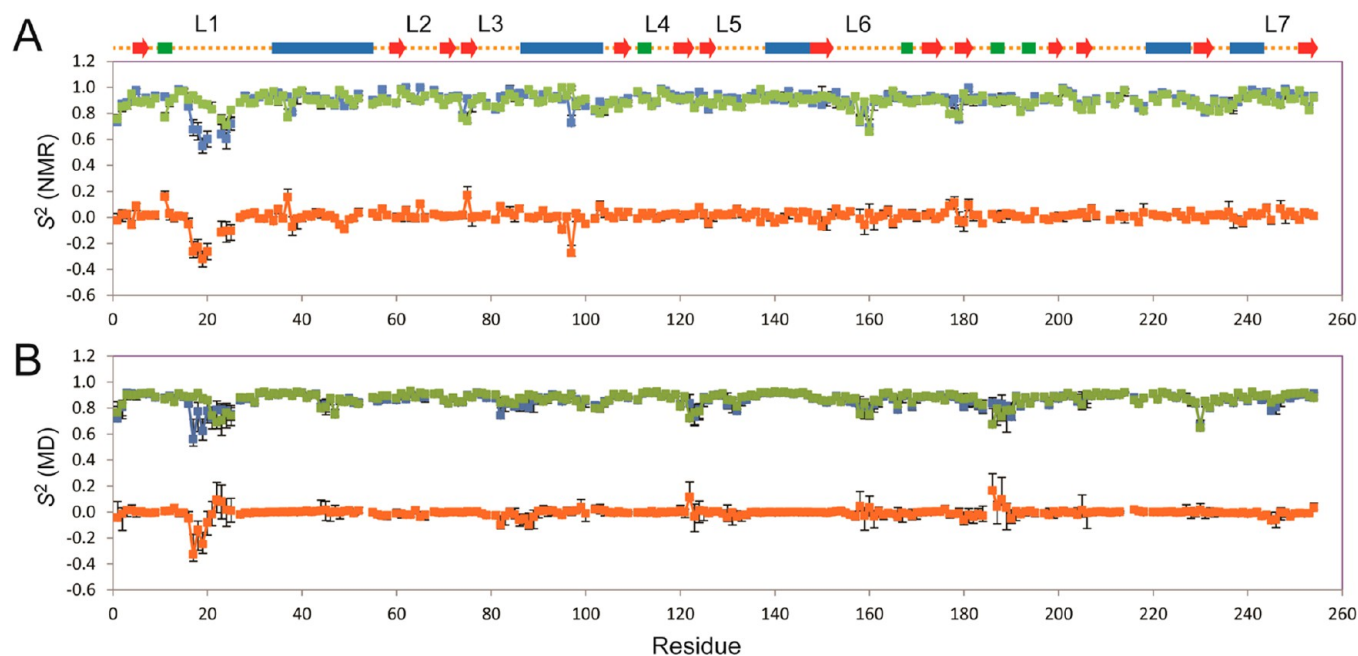

Figure 7. NMR and MD-derived order parameters for apo and L-citrulline-bound DM-PaDDAH. (A) Plots of the generalized order parameters S^2 for ^{15}N−^{1}H bond vector orientations obtained by model-free analysis of the multiple field ^{15}N R_1, R_2, and {^{1}H}^{15}N heteronuclear NOE data for apo (blue) and L-citrulline-saturated (green) DM-PaDDAH. (B) Plots of ^{15}N−^{1}H S^2 values obtained from multiple slices of molecular dynamics trajectories computed for apo (blue) and L-citrulline-saturated (green) DM-PaDDAH based upon the crystal structure coordinates PDB code 1H70. In both (A) and (B), the difference in S^2 values between the two states is plotted in orange. The secondary structure of PaDDAH is depicted at the top of the figure.
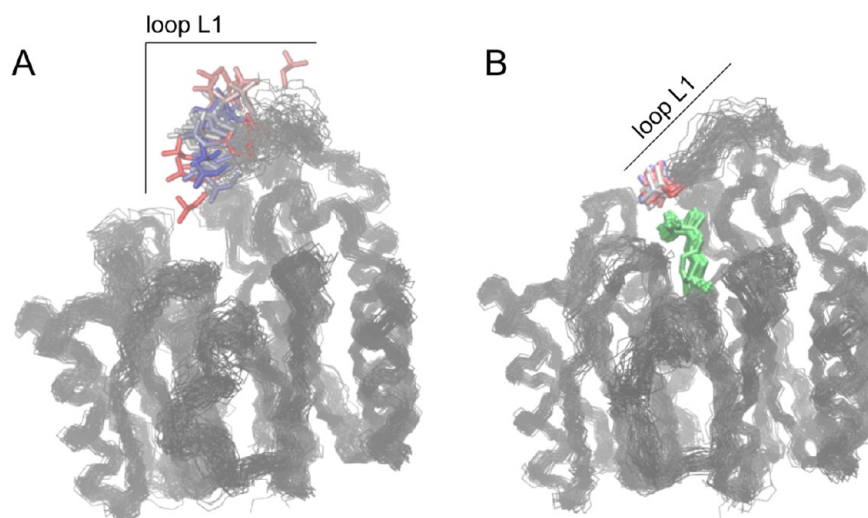
Figure 8. MD simulation of PaDDAH. Twenty-five equally spaced snapshots of 100 ns atomistic explicit solvent molecular dynamics trajectories computed for (A) apo DM-PaDDAH, and (B) L-citrulline bound DM-PaDDAH. The position of loop L1 is indicated in each case. The protein backbone atom coordinates have been best fit to the starting structure to eliminate the effects overall rotation and translation. L-Citrulline is shown in green. In each snapshot, the side chain of Leu18 in loop 1 is depicted in stick representation; red (start, 0 ns)-to-blue (100 ns) color gradation is used to indicate a sense of the time course of the simulation.

code 1H70) as a structural model, the analysis also showed that the degree of rotational diffusion anisotropy, predicted by the NMR measurements, is relatively small ($D_{\parallel}/D_{\perp} \sim 1.04$), broadly consistent the moments of inertia ratio $I_{xx}/I_{yy}/I_{zz} = 1.0:0.86:0.80$.

For apo DM-PaDDAH evidence of exchange contributions to ^{15}N R_2 (R_{ex}) was slight: the maximum values detected at 800 MHz were <5 s^{-1} with outlying, highest values identified for Phe2 in the N-terminus, Leu145, His162 in L6, and Thr165 (data not shown). On the other hand, following model-free analysis, the pattern of generalized order parameters (S^2) for NH bonds was broadly flat with values in the range 0.8−0.9, which are typical of highly ordered protein structure (Figure 7A). Exceptions were Phe2 at the extreme N-terminus of the protein, and Gly17-Ser20 and Leu23-Lys25 in loop L1, which display S^2 as low as 0.55, and Glu158 and Val160 in loop L6 (S^2 = 0.73 and 0.69, respectively).

For L-citrulline-saturated DM-PaDDAH, isolated instances of a significant exchange contribution to ^{15}N transverse relaxation from exchange (R_{ex}) at 800 MHz were detected for Thr71 (2.7 s^{-1}), Leu145 (7.0 s^{-1}), and Val160 (10.1 s^{-1}). The intensities of cross peaks for residues in the C-terminal portion of loop L6, comprising His162-Thr165, are relatively weak in the spectrum, suggesting the presence of residual ^{1}H exchange line broadening, and leading to an increase in the uncertainty in the heteronuclear NOE measurement due to the reduced signal-to-noise ratio. Following model-free analysis the profile of S^2 values for DM-PaDDAH saturated with L-citrulline was broadly flat at the level of $S^2 > 0.8$ for the majority of the length of the protein, with notable low values at Gly24 (S^2 = 0.71) in the C-terminal portion of loop L1 and Glu158 (S^2 = 0.74) and Val160 (S^2 = 0.66) in the N-terminal part of loop L6 (Figure 7A).

An essentially identical pattern of dynamics parameters was detected for apo and L-citrulline-bound TM-PaDDAH. Thus ligand binding to DM- and TM-PaDDAH leads to ordering of the N-terminal portion of loop L1, with quenching of the picosecond−nanosecond time scale motion that gives rise to low S^2 values in the ligand-free state. The fast motion associated with Gly24 in the C-terminal portion of loop L1 and residues

Glu158 and Val160 in the N-terminal part of loop L6 appeared to be unaffected by ligand binding, as these residues exhibited relatively low S^2 values in both the apo and L-citrulline bound states. Notably, these residues exhibited small but significant chemical shift changes in the presence of L-citrulline, but these perturbations were not as great as those shown by neighboring residues in loops L1 and L6 that were predicted from the crystal structure to be in direct contact with the ligand (e.g., Leu18 in L1 and His162 in L6).

Dynamics by Molecular Dynamics Simulation. To provide a real-space picture of the dynamic properties of PaDDAH, we performed atomistic, explicit solvent MD simulations of apo and L-citrulline-bound PaDDAH, based upon the X-ray coordinates of the protein/ligand complex. For the apo protein trajectories the L-citrulline coordinates were removed, and solvent water molecules were allowed to enter the binding site, both during the artificial solvation stage and throughout the energy minimization, equilibration, and production phases of simulation. Consistently during multiple simulations at 25 °C, the L1 loop was observed to detach from the main body of the protein and wander around relative to the rest of the protein without returning to its starting position (Figure 8A). On the other hand, for simulations with bound L-citrulline, the N-terminal part of the L1 loop remained close to its starting position. Of interest with respect to the description of the ligand coordination described in the introduction is the trajectory of Leu18 in the L1 loop. In the case of the ligand-bound protein, Leu18 remains essentially locked in van der Waals contacts with the bound L-citrulline with maintenance of the χ1 and χ2 torsion angles (Figure 8B). On the other hand in the case of the apo protein, the Leu18 side chain appeared to be almost unconstrained and could also adopt orientations that point further away from the main body of the protein (Figure 8A).

Representative MD simulation trajectories were used to predict the generalized order parameters for NH bond orientation (S^2)[20,21] for comparison with those derived from NMR relaxation measurements (Figure 7B). Notwithstanding the inherent limitations of the force field approximations, the
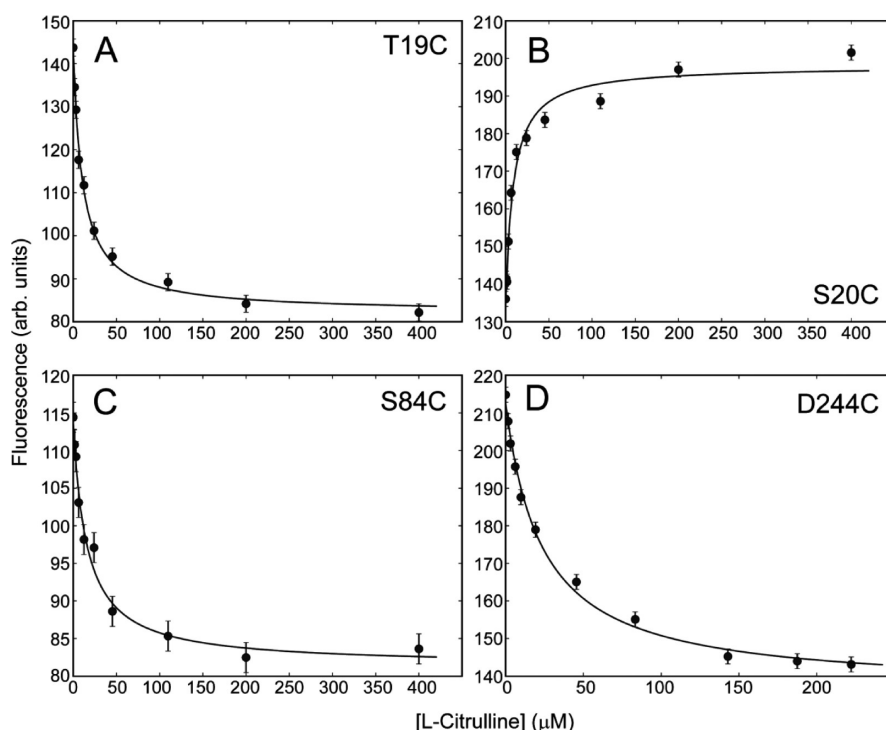
Figure 9. Change in fluorescence on titration of L-citrulline with MDCC-conjugated variants of TM-PaDDAH. Error bars reflect the standard error of multiple fluorescence measurements. Nonlinear least-squares fits were performed for: (A) MDCC-Thr19Cys DM-PaDDAH; (B) MDCC-Ser20Cys DM-PaDDAH; (C) MDCC-Ser84Cys DM-PaDDAH; and (D) MDCC-Asp244Cys DM-PaDDAH. The fitted values for the equilibrium dissociation constants are 10.8 ± 1.1 μM, 7.2 ± 1.6 μM, 15.7 ± 2.8 μM, and 23.5 ± 2.7 μM, respectively.
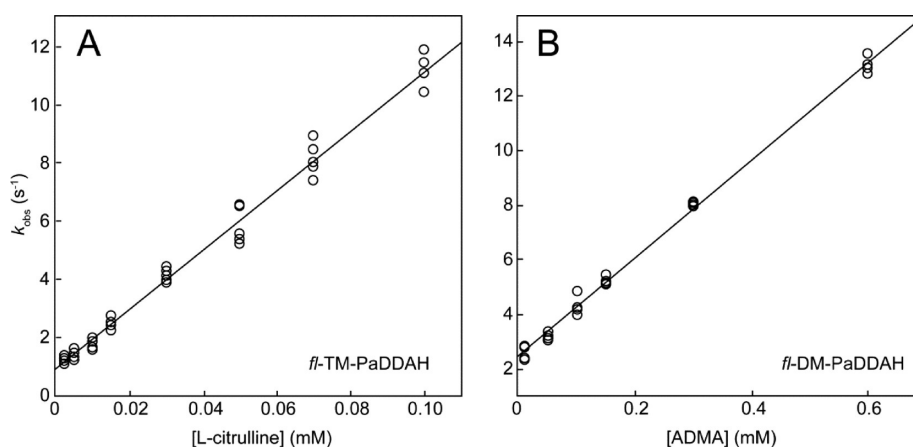

Figure 10. Time-resolved measurement of ligand binding to fluorescently labeled PaDDAH. Plots of the fitted apparent first-order rate constants k_{obs} for the time-dependent change in fluorescence emission filtered at 455 nm in multiple independent stopped-flow rapid mixing measurements of the interaction of (A) L-citrulline with MDCC-Ser20Cys TM-PaDDAH (fl-TM PaDDAH) and (B) ADMA with MDCC-Ser20Cys DM-PaDDAH (fl-DM PaDDAH). Least squares fitting (see Materials and Methods) yields for (A) $k_{off}^{(TM/L\text{-cit})} = 0.86$ s^{-1}, and $k_{on}^{(TM/L\text{-cit})} = 1.0 \times 10^5$ M^{-1} s^{-1}, and for (B) $k_{on}^{(DM/ADMA)} = 1.8 \times 10^5$ M^{-1} s^{-1} and $k_{off}^{(DM/ADMA)} + k_{cat} = 2.5$ s^{-1}.

overall profiles of measured and predicted S^2 values were broadly similar, consistent with other similar studies.[28,31,33−35] This suggested that the MD trajectory provided a realistic picture for the differential dynamics of the apo and ligand-bound states of PaDDAH, evidenced by the NMR measurements. MD-derived S^2 values included residues for which NMR measurements were not possible, for example, due to rapid NH/solvent exchange. Plotting the difference between the values for apo and L-citrulline-bound PaDDAH suggested that ligand binding quenched high-frequency, internal motion in the N-terminal portion of the L1 loop (ΔS^2 ∼0.33), accompanied

by relatively minor effects in some other parts of the protein chain (residues 88, 122, 187−189; $|\Delta S^2| < 0.17$).

Fluorescence Measurements. Combined NMR and MD analysis of PaDDAH showed that ligand binding was accompanied by a disorder-to-order transition for the L1 loop. This transition was characterized further by fluorescence, following chemical ligation of an environmentally sensitive diethylaminocoumarin fluorophore to a cysteine, introduced at specific locations by site-directed mutagenesis. The procedure adopted was essentially identical to that described for the bacterial actin homologue ParM.[36] Single cysteines were introduced at several sites in the TM-PaDDAH protein,

including Thr19Cys (L1), Ser20Cys (L1), Ser84Cys (L3), and Asp244Cys (L7). In each case, the fluorescent MDCC label was coupled to the protein. MDCC did not couple to the "wild-type" TM-PaDDAH protein at all, consistent with the wild-type Cys residues (Cys45, Cys70, Cys74, Cys205) being buried. Each of the fluorophore-labeled proteins was titrated with L-citrulline, following the change in fluorescence as shown in Figure 9. The fluorescence intensity either increased (Ser20Cys) or decreased (Thr19Cys, Ser84Cys, Asp244Cys) in the presence of L-citrulline. This suggested that, while in each case the fluorophore was sensitive to occupation of the TM-PaDDAH binding site, the nature of the change in the environment of the fluorophore was dependent upon the site of modification. In each case, the dissociation constant was in the low micromolar range. The value for MDCC-Ser20Cys TM-PaDDAH, $7.2 \pm 1.6\ \mu$M, was only 2-fold higher than that obtained by heteronuclear NMR with unlabeled TM-PaDDAH (3.5 μM, see above). The titration with MDCC-Ser20Cys TM-PaDDAH was accompanied by an increase in MDCC fluorescence, consistent with the fluorophore moving from a relatively solvent-exposed position in the apo state to a more buried location upon L-citrulline binding. Thus, PaDDAH, labeled at the Ser20Cys site in L1, provided a probe that behaved in a manner consistent with ligand-dependent ordering of the L1 loop, perhaps driven by contact of the neighboring Leu18 side chain with L-citrulline, as suggested in the MD simulations. However, there was no fluorescence change for ADMA interaction with MDCC-Ser20Cys-MDCC TM-PaD-DAH (*fl*-TM-PaDDAH), suggesting that affinity of this DDAH substrate for this catalytically inactive (Cys249Ser) variant was weak.

L-Citrulline was mixed with *fl*-TM-PaDDAH under pseudo-first-order conditions and the time course of fluorescence followed. There was a systematic rise in fluorescence emission with monoexponential behavior (Figure 3 of the Supporting Information). The kinetics were measured over a range of L-citrulline concentrations (Figure 10A). The dependence of k_{obs} on concentration was linearly fitted for the TM-PaDDAH/L-citrulline association reaction (see Materials and Methods), yielding $k_{off}^{(TM/L\text{-}cit)} = 0.86\ s^{-1}$, and $k_{on}^{(TM/L\text{-}cit)} = 1.0 \times 10^5\ M^{-1}\ s^{-1}$. The predicted equilibrium dissociation constant, $K_D^{(TM/L\text{-}cit)}\ (= k_{off}^{(TM/L\text{-}cit)}/k_{on}^{(TM/L\text{-}cit)})$ was 8.4 μM.

Conversely with MDCC-Ser20Cys DM-PaDDAH (*fl*-DM-PaDDAH), there was no signal for binding L-citrulline, consistent with the very weak interaction that was observed by NMR at higher protein and ligand concentrations. However, there was a fluorescence response to binding substrate, ADMA, and its time course was measured by stopped-flow fluorescence. Several stopped-flow traces were recorded for different concentrations of ADMA under pseudo-first-order conditions (Figure 10B). Because *fl*-DM-PaDDAH retains the critical catalytic Cys249 residue, it was expected to convert ADMA to L-citrulline and dimethylamine (DMA). The data were then analyzed in terms of a Michaelis−Menten enzyme reaction scheme (see Materials and Methods). The plot of the k_{obs} against ADMA concentration yielded an essentially straight line graph (Figure 10B). Least-squares fitting gave $k_{on}^{(DM/ADMA)}$ as $1.8 \times 10^5\ M^{-1}\ s^{-1}$ and $k_{off}^{(DM/ADMA)} + k_{cat} = 2.5\ s^{-1}$. Assuming $k_{cat} = 0.5\ s^{-1}$, as estimated previously for the unmodified DM-PaDDAH,[10] $k_{off}^{(DM/ADMA)} = 2.0\ s^{-1}$, and the predicted equilibrium dissociation constant for *fl*-DM-PaDDAH binding to ADMA $K_D^{(DM/ADMA)}\ (= k_{off}^{(DM/ADMA)}/k_{on}^{(DM/ADMA)}) = 110\ \mu$M.

■ DISCUSSION

NMR and fluorescence methods were used to probe the effects of ligand binding to both active and catalytically inactive (Cys249Ser) variants of bacterial DDAH. The combination of chemical shift assignments and heteronuclear relaxation measurements indicate that the protein maintains its overall $\beta\beta\alpha\beta$-propeller fold in both apo and ligand-bound states. Furthermore, it behaves as a pseudospherical monomer with rotational correlation time of 14 ns, consistent with computer predictions of the hydrodynamic characteristics, using the crystallographic coordinates of the L-citrulline-bound protein.

Substrate binding to active DM-PaDDAH was accompanied by conversion to L-citrulline, which binds to the enzyme with relatively weak affinity, $K_D^{(DM/L\text{-}cit)} = 3.6$ mM as measured by NMR. This value is in reasonable agreement to that obtained by colorimetric inhibition kinetics for the wild-type protein $(K_i^{(L\text{-}cit)} = 8.4\ mM)$.[37] Although TM-PaDDAH was previously assumed to be inactive, the slow conversion of ADMA to DMA and L-citrulline was observed by 1D ^{1}H NMR in the presence of high concentration of TM-PaDDAH over a period of hours. This reaction was likely to be due to the presence of a very low catalytic activity of the mutant enzyme ($\sim$0.04 h^{-1}). Similar instances of residual activity of enzymes mutated at "essential" residues have been documented elsewhere[38] reflecting the fact that the "inactive" site of such variants can still retain properties that lower the activation barrier to substrate conversion, albeit to a lesser degree than for the wild type. Consistent with this interpretation, this activity only occurred significantly at the high concentration of TM-PaDDAH required for multidimensional NMR experiments. When ADMA was added to low concentrations of TM-PaDDAH in fluorescence experiments, there was no evidence of substrate binding or turnover.

It has been suggested that ADMA binding to PaDDAH is accompanied by substrate-assisted deprotonation of the active site Cys249 thiol group, such that the positive charge of the buried dimethylguanidinium group is balanced by the negative charge of the induced Cys thiolate.[39] From our time-resolved fluorescence measurement with *fl*-DM-PaDDAH, an apparent dissociation constant for the interaction of ADMA $(K_D^{(DM/ADMA)})$ was obtained, indicating binding is 30-fold tighter than for the reaction product, L-citrulline. This difference may be due to the electrostatic interaction between the complementary charges of the ADMA guanidinium moiety and Cys249 thiolate contributing to the binding energy. The identity of the conjugate base that is responsible for the removal of the Cys249 thiol proton in the presence of substrate remains elusive.[39]

In contrast L-citrulline binds relatively tightly to TM-PaDDAH with $K_D^{(TM/L\text{-}cit)}$ being 3.5 μM, as measured by NMR titration. Consistent with this, L-citrulline binds to a series of fluorescently labeled TM-PaDDAH variants with dissociation constants in the low micromolar range, as assessed in both static (Figure 9) and time-dependent (Figure 10B) measurements. The PaDDAH Cys249 pKa is reported to be 8.8 in the absence of ligand.[39] Replacement of Cys249 with Ser in TM-PaDDAH substitutes the Cys thiol with a Ser hydroxyl group with a significantly higher pK_a. Therefore, the hydroxyl proton is not likely to be removed in the presence of a positively charged substrate by the same mechanism that can take place with Cys in this position. This gives the active site an electrostatic profile that is more resistant to binding the substrate ADMA, since the Ser residue cannot be deprotonated

to make a favorable interaction with the positively charged methylguanidinium group but apparently is better able to bind neutral L-citrulline: $K_D^{(TM/L\text{-}cit)}$ is 3.6 μM as measured by NMR or 8.4 μM by measuring binding kinetics for MDCC-Ser20Cys TM-PaDDAH.

The heteronuclear relaxation measurements provide a picture of apo DM-PaDDAH that exhibits relatively little internal motion. A clear exception to this characterization is reflected in the NH bond S^2 order parameters, which report on "fast" internal motion, for the residues of loop L1 (Figure 7A). The lowest value of S^2 is 0.55 for Thr19, well outside of the range typically associated with ordered protein structure. This result, combined with the fact that NH cross peaks of two other L1 residues are not detected in the NMR experiments, suggests that the L1 region is dynamically disordered on the pico- to nanosecond time scale. Upon the basis of a starting model, derived from the PaDDAH crystal structure from which the L-citrulline has been removed, the unbiased MD simulation of DM-PaDDAH provides a visual representation of the nanosecond time scale dynamics of the protein. The profile of S^2 order parameters, predicted by the MD trajectories, is similar to that obtained experimentally, despite the known limitations of the MD force fields.[31] The MD results therefore provide both a qualitative (Figure 8) and quantitative (Figure 7B) picture of the internal motion of the protein. Thus, as Figure 8A demonstrates, in the apo protein the L1 loop displays a high degree of flexibility relative to the rest of the protein. In particular, both the backbone and side chain of Leu18 move away from the body of the protein, providing an uninterrupted access channel to the active site.

In contrast in the presence of excess L-citrulline ligand, the profile of NMR-derived S^2 order parameters possesses an even lower level of variance than for apo DM-PaDDAH. Notably, the low S^2 values in the L1 loop region are elevated to normal levels, suggesting that in the bound protein the fast time scale internal motion is largely quenched. This characteristic is recapitulated in the MD simulations as depicted in Figures 7B and 8B, where the range of conformational states adopted by the L1 loop is extremely limited compared to that exhibited in the case of the apo protein. In particular, the position of Leu18 is essentially fixed, and the side chain remains in van der Waals contact with the L-citrulline throughout. Importantly, ^{15}N relaxation analysis of either apo and L-citrulline-bound TM-PaDDAH, a complex that exhibits much slower dissociation kinetics, shows an essentially identical picture of ligand-dependent L1 dynamics to DM-PaDDAH. Intriguingly, in the human DDAH-1 protein, substitution of Leu30 which corresponds to Leu18 in PaDDAH with alanine raises the substrate K_M 10-fold.[40] This highlights the importance of this evolutionarily conserved residue for ligand interaction.

The observation that the L1 loop undergoes an apparent disorder-to-order transition upon ligand binding led us to consider whether we could exploit this behavior to develop a fluorescence reporter of L-citrulline. It is possible that the rate determining step of the DDAH reaction mechanism is release of the L-citrulline product limited by the opening rate of the L1 loop. Development of an in situ reporter of the presence of L-citrulline compatible with time-resolved fluorescence measurements would enable us to address this possibility. To these ends we built upon previous work[36,41] and conjugated the environmentally sensitive fluorescent label, MDCC, to Cys residues introduced into various positions in the ligand binding loops of DM- and TM-PaDDAH.

The fluorescence of the TM-PaDDAH conjugates is sensitive to the presence of L-citrulline (Figure 9). In the case of the Cys20-MDCC-conjugated TM-PaDDAH, the fluorescence increased, consistent with L-citrulline binding causing closure of the L1-loop and introducing interactions of the fluorophore with the protein surface. For the other three conjugates tested, namely, Thr19Cys-, Ser84Cys-, and Asp244Cys-, L-citrulline induced a decrease in emission intensity, perhaps consistent with ligand binding causing a rearrangement that effects higher solvent exposure of the coumarin. A full rationalization of the fluorescence behavior would require detailed, structural studies of the apo and bound states of the fluorescence conjugates. Nevertheless, these results suggest that such reagents might provide the basis for further development of a protein-based optical sensor for L-citrulline at micromolar concentrations, a level that is appropriate to the range in which L-citrulline may behave as a biomarker of diseases of the human gut.[42] To our knowledge, measurement of L-citrulline concentration is currently obtained by one of two methods: either a somewhat laborious colorimetric reaction[43,44] that can be confounded by the presence of other uriedyl-group containing compounds and some other common reagents (sucrose and guanidinium chloride) or by amino acid analysis or hybrid liquid chromatography (LC)-mass spectrometry and LC-laser-induced fluorescence methods that require expensive instrumentation.

The fluorescence signal was used to measure the kinetic parameters for the interaction of ADMA and L-citrulline with Ser20Cys-MDCC DM- and TM-PaDDAH. From the stopped-flow measurements $k_{on}^{(TM/L\text{-}cit)} = 1.0 \times 10^5$ M^{-1} s^{-1} and $k_{on}^{(DM/ADMA)} = 1.8 \times 10^5$ M^{-1} s^{-1}. However, as discussed above, L-citrulline binding to DM-PaDDAH could not be measured by this technique, but an NMR titration gives $K_D^{(DM/L\text{-}cit)} = 3.6$ mM. An estimate of $k_{off}^{(DM/L\text{-}cit)}$ is possible by combining this number and an estimate of $k_{on}^{(DM/L\text{-}cit)}$. Assuming $k_{on}^{(DM/L\text{-}cit)}$ is similar to $k_{on}^{(TM/L\text{-}cit)}$ and $k_{on}^{(DM/ADMA)}$, then $k_{off}^{(DM/L\text{-}cit)}$ is predicted to be $\sim$500 s^{-1}. This value is $\sim$1000-fold higher than the turnover number for the enzyme, indicating in turn that the rate limiting step is not product release or lid-opening. Moreover for lid-opening to be rate determining, then the true value of $k_{on}^{(DM/L\text{-}cit)}$ would need to be $\sim$100 M^{-1} s^{-1}, which is so small as to be extremely unlikely. The rate determining step of the DDAH reaction must therefore be represented by an earlier "chemical" step in the mechanism.[9,39]

In this study, we have characterized the equilibrium and kinetic aspects of the interaction of substrate and reaction products with PaDDAH, alongside both experimental measurement and computer simulation of the molecular dynamics of apo and citrulline-bound proteins. Overall the picture that emerges is that the lid to the active site chamber of PaDDAH, represented by loop L1, is highly dynamic in the apo state to facilitate substrate access. The lid is demonstrably more ordered in the ligand bound state, in part as a result of contact between the resident ligand and L1 loop residues, yet the opening rate of the lid is much faster than the overall reaction rate for the enzyme-catalyzed reaction, suggesting that the lid can detach from and rebind the bound reaction product L-citrulline. It is difficult to assess whether the L1 loop is more strongly constrained during the intermediate steps of the reaction mechanism, such as during the lifetime of the putative covalent thiouronium intermediate that is formed concomitant with the scission of the substrate C^ζ–N^η bond.[39,45] Potentially the flexibility of the loop allows the exchange of the released

dimethylamine coproduct for a water molecule that is required for the hydrolysis of the intermediate, though there may be other exit routes for this as it is the smaller of the reaction products, for example, via a narrow opening between Leu161, Thr165, and Gly245. However, our conclusion that chemistry (not product release) is the rate-limiting step would be in agreement with earlier findings in which the covalent thiouronium intermediate accumulates and is trapped in reactions during steady-state turnover.[39,45]

The fluorophore-TM-PaDDAH conjugates described in this work provide a platform for the development of a protein-based sensor of L-citrulline: the immediate aim of such work would be to enhance the signal-to-noise ratio of the fluorescence change and to measure the ligand selectivity. Given the rather unusual pentein propeller fold of DDAH, and the coordination of bound ligand which appears to depend upon specific H-bonding arrangement of the α-amino and -carboxylate groups, it is intriguing to consider whether protein design or directed evolution methods could be used to develop DDAH-based sensors for other amino acids.

■ ASSOCIATED CONTENT

ⓢ Supporting Information
[15]N nuclear relaxation measurements for apo TM-PaDDAH (Figure S1), ^{15}N nuclear relaxation measurements for L-citrulline-saturated TM-PaDDAH (Figure S2), and representative time-resolved stopped-flow fluorescence traces for MDCC-labeled DM-PaDDAH with ADMA (Figure S3). This material is available free of charge via the Internet at http://pubs.acs.org.

Accession Codes
Backbone chemical shift assignments and ^{15}N nuclear relaxation rates described herein have been deposited in the BioMagResBank: accession numbers 19743, 19744, 19615, and 19616.

■ AUTHOR INFORMATION

Corresponding Author
*E-mail: pdrisco@nimr.mrc.ac.uk. Phone: +44 (0)20 8816 2061. Fax: +44 (0)20 8906 4477.

Notes
The authors declare no competing financial interest.

■ ACKNOWLEDGMENTS

■ ABBREVIATIONS

ADMA, asymmetric N^{η},N^{η}-dimethylarginine; AUC, analytical ultracentrifugation; DDAH, dimethylarginine dimethylamino-hydrolase; DM, double mutant; DTT, dithiothreitol; *fl*-, MDCC-Ser20Cys fluorescently labeled-; hNOE, heteronuclear Overhouser effect; L-cit, L-citrulline; L-NMMA, L-N^{η}-mono-methylarginine; MD, molecular dynamics; MDCC, N-[2-(1-maleimidyl)ethyl]-7-(diethylamino)coumarin-3-carboxamide; NMR, nuclear magnetic resonance; NOS, nitric oxide synthase; NPT, constant atom number, pressure and temperature; PaDDAH, *Pseudomonas aeruginosa* DDAH; TM, triple mutant

■ REFERENCES

(1) Leiper, J., and Nandi, M. (2011) The therapeutic potential of targeting endogenous inhibitors of nitric oxide synthesis. *Nat. Rev. Drug Discovery 10*, 277−291.

(2) Linsky, T., Wang, Y., and Fast, W. (2011) Screening for Dimethylarginine Dimethylaminohydrolase Inhibitors Reveals Ebselen as a Bioavailable Inactivator. *ACS Med. Chem. Lett. 2*, 592−596.

(3) Linsky, T. W., and Fast, W. (2012) Discovery of structurally-diverse inhibitor scaffolds by high-throughput screening of a fragment library with dimethylarginine dimethylaminohydrolase. *Bioorg. Med. Chem. 20*, 5550−5558.

(4) Lluis, M., Wang, Y., Monzingo, A. F., Fast, W., and Robertus, J. D. (2011) Characterization of C-Alkyl Amidines as Bioavailable Covalent Reversible Inhibitors of Human DDAH-1. *ChemMedChem 6*, 81−88.

(5) Leiper, J., Nandi, M., Torondel, B., Murray-Rust, J., Malaki, M., O'Hara, B., Rossiter, S., Anthony, S., Madhani, M., Selwood, D., Smith, C., Wojciak-Stothard, B., Rudiger, A., Stidwill, R., McDonald, N. Q., and Vallance, P. (2007) Disruption of methylarginine metabolism impairs vascular homeostasis. *Nat. Med. 13*, 198−203.

(6) Thiemermann, C. (1997) Nitric oxide and septic shock. *Gen. Pharmacol. 29*, 159−166.

(7) Cuzzocrea, S., Chatterjee, P. K., Mazzon, E., McDonald, M. C., Dugo, L., Serraino, I., Caputi, A. P., and Thiemermann, C. (2002) Beneficial effects of GW274150, a novel, potent and selective inhibitor of iNOS activity, in a rodent model of collagen-induced arthritis. *Eur. J. Pharmacol. 18*, 119−129.

(8) Thomsen, L. L., and Miles, D. W. (1998) Role of nitric oxide in tumour progression: Lessons from human tumours. *Cancer Metastasis Rev. 17*, 107−118.

(9) Murray-Rust, J., Leiper, J., McAlister, M., Phelan, J., Tilley, S., Maria, J. S., Vallance, P., and McDonald, N. (2001) Structural insights into the hydrolysis of cellular nitric oxide synthase inhibitors by dimethylarginine dimethylaminohydrolase. *Nat. Struct. Biol. 8*, 679−683.

(10) Magalhaes, B. S., Harris, R. E., Plevin, M. J., and Driscoll, P. C. (2004) Letter to the Editor: Backbone (1)H, (13)C, and (15)N resonance assignments for a 29 kD monomeric variant of Pseudomonas aeruginosa dimethylarginine dimethylaminohydrolase. *J. Biomol. NMR 29*, 463−464.

(11) Plevin, M. J., Magalhaes, B. S., Harris, R., Sankar, A., Perkins, S. J., and Driscoll, P. C. (2004) Characterization and manipulation of the *Pseudomonas aeruginosa* dimethylarginine dimethylaminohydrolase monomer-dimer equilibrium. *J. Mol. Biol. 341*, 171−184.

(12) Bax, A., and Grzesiek, S. (1993) Methodological Advances in Protein NMR. *Acc. Chem. Res. 26*, 131−138.

(13) Kay, L. E., Torchia, D. A., and Bax, A. (1989) Backbone Dynamics of Proteins as Studied by N-15 Inverse Detected Heteronuclear NMR-Spectroscopy - Application to Staphylococcal Nuclease. *Biochemistry 28*, 8972−8979.

(14) Farrow, N. A., Muhandiram, R., Singer, A. U., Pascal, S. M., Kay, C. M., Gish, G., Shoelson, S. E., Pawson, T., Formankay, J. D., and Kay, L. E. (1994) Backbone Dynamics of a Free and a Phosphopeptide-Complexed Src Homology-2 Domain Studied by N-15 NMR Relaxation. *Biochemistry 33*, 5984−6003.

(15) Piotto, M., Saudek, V., and Sklenar, V. (1992) Gradient-Tailored Excitation for Single-Quantum NMR-Spectroscopy of Aqueous-Solutions. *J. Biomol. NMR 2*, 661−665.

(16) Grzesiek, S., and Bax, A. (1993) The Importance of Not Saturating H_2O in Protein NMR - Application to Sensitivity Enhancement and NOE Measurements. *J. Am. Chem. Soc. 115*, 12593−12594.

(17) Delaglio, F., Grzesiek, S., Vuister, G. W., Zhu, G., Pfeifer, J., and Bax, A. (1995) NMRPIPE - a Multidimensional Spectral Processing System Based on Unix Pipes. *J. Biomol. NMR 6*, 277−293.

(18) Fogh, R. H., Boucher, W., Vranken, W. F., Pajon, A., Stevens, T. J., Bhat, T. N., Westbrook, J., Ionides, J. M. C., and Laue, E. D. (2005) A framework for scientific data modeling and automated software development. *Bioinformatics 21*, 1678−1684.

(19) Vranken, W. F., Boucher, W., Stevens, T. J., Fogh, R. H., Pajon, A., Llinas, P., Ulrich, E. L., Markley, J. L., Ionides, J., and Laue, E. D. (2005) The CCPN data model for NMR spectroscopy: Development of a software pipeline. *Proteins 59*, 687−696.

(20) Lipari, G., and Szabo, A. (1982) Model-Free Approach to the Interpretation of Nuclear Magnetic-Resonance Relaxation in Macro-molecules 1. Theory and Range of Validity. *J. Am. Chem. Soc. 104*, 4546−4559.

(21) Lipari, G., and Szabo, A. (1982) Model-Free Approach to the Interpretation of Nuclear Magnetic-Resonance Relaxation in Macro-molecules. 2. Analysis of Experimental Results. *J. Am. Chem. Soc. 104*, 4559−4570.

(22) Blackledge, M., Cordier, F., Dosset, P., and Marion, D. (1998) Precision and uncertainty in the characterization of anisotropic rotational diffusion by N-15 relaxation. *J. Am. Chem. Soc. 120*, 4538−4539.

(23) Mandel, A. M., Akke, M., and Palmer, A. G. (1995) Backbone Dynamics of *Escherichia coli* Ribonuclease H1 - Correlations with Structure and Function in an Active Enzyme. *J. Mol. Biol. 246*, 144−163.

(24) Palmer, A. G., Rance, M., and Wright, P. E. (1991) Intramolecular Motions of a Zinc Finger DNA-Binding Domain from Xfin Characterized by Proton-Detected Natural Abundance C-12 Heteronuclear NMR-Spectroscopy. *J. Am. Chem. Soc. 113*, 4371−4380.

(25) Koradi, R., Billeter, M., and Wuthrich, K. (1996) MOLMOL: A program for display and analysis of macromolecular structures. *J. Mol. Graphics 14*, 51−55.

(26) Case, D. A., Cheatham, T. E., Darden, T., Gohlke, H., Luo, R., Merz, K. M., Onufriev, A., Simmerling, C., Wang, B., and Woods, R. J. (2005) The AMBER biomolecular simulation programs. *J. Comput. Chem. 26*, 1668−1688.

(27) Pearlman, D. A., Case, D. A., Caldwell, J. W., Ross, W. S., Cheatham, T. E., Debolt, S., Ferguson, D., Seibel, G., and Kollman, P. (1995) AMBER, a Package of Computer-Programs for Applying Molecular Mechanics, Normal-Mode Analysis, Molecular-Dynamics and Free-Energy Calculations to Simulate the Structural and Energetic Properties of Molecules. *Comput. Phys. Commun. 91*, 1−41.

(28) Trbovic, N., Kim, B., Friesner, R. A., and Palmer, A. G. (2008) Structural analysis of protein dynamics by MD simulations and NMR spin-relaxation. *Proteins 71*, 684−694.

(29) Dupradeau, F. Y., Pigache, A., Zaffran, T., Savineau, C., Lelong, R., Grivel, N., Lelong, D., Rosanski, W., and Cieplak, P. (2010) The R.E.D. tools: advances in RESP and ESP charge derivation and force field library building. *Phys. Chem. Chem. Phys. 12*, 7821−7839.

(30) Vanquelef, E., Simon, S., Marquant, G., Garcia, E., Klimerak, G., Delepine, J. C., Cieplak, P., and Dupradeau, F. Y. (2011) RED Server: a web service for deriving RESP and ESP charges and building force field libraries for new molecules and molecular fragments. *Nucleic Acids Res. 39*, W511−W517.

(31) Zeiske, T., Stafford, K. A., Friesner, R. A., and Palmer, A. G. (2013) Starting-structure dependence of nanosecond timescale intersubstate transitions and reproducibility of MD-derived order parameters. *Proteins 81*, 499−509.

(32) Corrie, J. E. T. (1994) Thiol-Reactive Fluorescent-Probes for Protein Labeling. *J. Chem. Soc. Perkin Trans. 1*, 2975−2982.

(33) MacRaild, C. A., Daranas, A. H., Bronowska, A., and Homans, S. W. (2007) Global changes in local protein dynamics reduce the entropic cost of carbohydrate binding in the arabinose-binding protein. *J. Mol. Biol. 368*, 822−832.

(34) Maragakis, P., Lindorff-Larsen, K., Eastwood, M. P., Dror, R. O., Klepeis, J. L., Arkin, I. T., Jensen, M. O., Xu, H. F., Trbovic, N., Friesner, R. A., Palmer, A. G., and Shaw, D. E. (2008) Microsecond molecular dynamics simulation shows effect of slow loop dynamics on backbone amide order parameters of proteins. *J. Phys. Chem. B 112*, 6155−6158.

(35) Long, D., Li, D. W., Walter, K. F., Griesinger, C., and Bruschweiler, R. (2011) Toward a predictive understanding of slow methyl group dynamics in proteins. *Biophys. J. 101*, 910−915.

(36) Kunzelmann, S., and Webb, M. R. (2009) A Biosensor for Fluorescent Determination of ADP with High Time Resolution. *J. Biol. Chem. 284*, 33130−33138.

(37) Stone, E. M., and Fast, W. (2005) A continuous spectrophoto-metric assay for dimethylarginine dimethylaminohydrolase. *Anal. Biochem. 343*, 335−337.

(38) Peracchi, A. (2001) Enzyme catalysis: removing chemically "essential" residues by site-directed mutagenesis. *Trends Biochem. Sci. 26*, 497−503.

(39) Stone, E. M., Costello, A. L., Tierney, D. L., and Fast, W. (2006) Substrate-assisted cysteine deprotonation in the mechanism of dimethylargininase (DDAH) from Pseudomonas aeruginosa. *Biochemistry 45*, 5618−5630.

(40) Wang, Y., Monzingo, A. F., Hu, S. G., Schaller, T. H., Robertus, J. D., and Fast, W. (2009) Developing Dual and Specific Inhibitors of Dimethylarginine Dimethylaminohydrolase-1 and Nitric Oxide Synthase: Toward a Targeted Polypharmacology To Control Nitric Oxide. *Biochemistry 48*, 8624−8635.

(41) Hirshberg, M., Henrick, K., Haire, L. L., Vasisht, N., Brune, M., Corrie, J. E. T., and Webb, M. R. (1998) Crystal structure of phosphate binding protein labeled with a coumarin fluorophore, a probe for inorganic phosphate. *Biochemistry 37*, 10381−10385.

(42) Bahri, S., Zerrouk, N., Aussel, C., Moinard, C., Crenn, P., Curis, E., Chaumeil, J. C., Cynober, L., and Sfar, S. (2013) Citrulline: from metabolism to therapeutic use. *Nutrition 29*, 479−484.

(43) Knipp, M., and Vasak, M. (2000) A colorimetric 96-well microtiter plate assay for the determination of enzymatically formed citrulline. *Anal. Biochem. 286*, 257−264.

(44) Boyde, T. R., and Rahmatullah, M. (1980) Optimization of conditions for the colorimetric determination of citrulline, using diacetyl monoxime. *Anal. Biochem. 107*, 424−431.

(45) Stone, E. A., Person, M. D., Costello, N. J., and Fast, W. (2005) Characterization of a transient covalent adduct formed during dimethylarginine dimethylaminohydrolase catalysis. *Biochemistry 44*, 7069−7078.